

Microstructure and Mechanical Properties of $\text{Co}_{21}\text{Cr}_{22}\text{Cu}_{22}\text{Fe}_{21}\text{Ni}_{14}$ Processed by High Pressure Torsion and Annealing

NOKEUN PARK ^{1,2,4}, XIANG LI,^{2,5} and NOBUHIRO TSUJI^{2,3,6}

1.—School of Materials Science and Engineering, Yeungnam University, Gyeongsan 38541, Republic of Korea. 2.—Department of Materials Science and Engineering, Kyoto University, Yoshida Honmachi, Sakyo-ku, Kyoto 606-8501, Japan. 3.—Elements Strategy Initiative for Structural Materials (ESISM), Kyoto University, Yoshida Honmachi, Sakyo-ku, Kyoto 606-8501, Japan. 4.—e-mail: nokeun_park@yu.ac.kr. 5.—e-mail: li.xiang.63c@st.kyoto-u.ac.jp. 6.—e-mail: nobuhiro-tsuji@mtl.kyoto-u.ac.jp

The strengthening mechanisms of $\text{Co}_{21}\text{Cr}_{22}\text{Cu}_{22}\text{Fe}_{21}\text{Ni}_{14}$ multiple-principal element alloy processed by high pressure torsion (HPT) and annealing were examined. Two face-centered cubic (FCC) phases were observed in the as-cast alloy; one was a Cu-rich phase and the other was a Cu-lean one. In the HPT process, the microhardness increased from 190 HV to 470 HV at a strain of 157 due to strain hardening and grain refinement hardening. X-ray diffraction showed that the lattice parameters of the two FCC phases became closer to each other at higher HPT strain, indicating the alloying of Cu into the Cu-lean matrix. The HPT processed specimens were annealed at 500°C, 550°C, 600°C, and 650°C. The microhardness increased to 540 HV after annealing at temperatures lower than 650°C, whereas it decreased when the specimen was annealed at 650°C. The mean grain size of the specimens annealed at temperatures lower than 650°C was much smaller than 100 nm, and Cu-rich clusters with sizes ranging from 2 nm to 32 nm were distributed homogeneously. The reasons for the formation of the Cu-rich nano-clusters were discussed from a perspective of the positive mixing enthalpy of Cu in the alloy and thermal energy for Cu diffusion at a given temperature. The dissolution and partitioning of two FCC phases played a key role in strengthening the $\text{Co}_{21}\text{Cr}_{22}\text{Cu}_{22}\text{Fe}_{21}\text{Ni}_{14}$ system.

INTRODUCTION

The properties (such as strength, elongation, corrosion resistance, magnetic property, *etc.*) of metallic materials, such as steels, aluminum alloys, magnesium alloys, *etc.*, can be controlled by adding relatively small fractions of different elements into the base metals. A series of studies of conventional alloys have increased our understanding of the various effects of alloying elements in metallic materials. On the other hand, a considerable challenge to the conventional concept of alloys occurred in 2004 when Yeh et al. designed new systems composed of many elements (at least five species) with almost equiatomic fractions.¹ This system did not have a major element (base metal); all the elements were both solutes and solvents, which is

completely different from the concept of conventional alloys designed previously. After Yeh et al.'s attempt, many researchers have examined multiple-principal elements alloys (MPEA) consisting of almost equiatomic compositions, which were called high-entropy alloys (HEA).^{1–14}

One important issue in MPEA is to predict the phases at a given chemical composition and temperature. Hume-Rothery's theory, which considers the difference in atomic size, relative valence, electronegativity, and electron concentration, has been used to predict the solubility in binary systems.^{8,15} The Hume-Rothery rule is still applied to predict the formation of a single phase in MPEA, where two factors are used mainly for the prediction: the mixing enthalpy and the atomic size difference.^{2–4,8,15,16} Combining these two factors makes it possible to

predict the formation of a single phase at a given temperature and chemical composition. A few systems consisting of a single phase solid solution without any second phases have been found, such as CoCrFeMnNi and CoCrCuFeNi systems.⁸ Although there have been some attempts to develop thermodynamic databases for MPEA systems, they are not yet fully acceptable and still under evolution.^{17–19}

MPEA are attractive materials because they exhibit novel mechanical properties, such as excellent strength, large capability for plastic deformation and great toughness.^{4–8,10–12} So far, however, most studies of MPEA systems have focused on making the alloys themselves or investigating their properties in the as-cast state. Two of the physical phenomena in MPEA reported by us previously were the deformation and recrystallization behaviors in the CoCrCuFeNi FCC system during conventional cold-rolling and subsequent annealing.^{20,21} Interestingly, the strength of the partially recrystallized specimen was much higher than the values predicted by the simple rule of mixtures. In addition, recrystallization of the 90% cold-rolled alloy was fairly slow. One of the reasons for making the situation complicated in the previous study was the existence of a second FCC phase. A Cu-rich FCC phase in a FCC matrix was observed in the as-cast CoCrCuFeNi alloy, and the Cu-rich second phase was elongated along the rolling direction by cold-rolling, making a laminated structure.²⁰ In addition, mechanical alloying can make a supersaturated solid solution.^{22–25} So-called severe plastic deformation (SPD), where huge plastic strains are applied to bulky metallic materials, can realize mechanical alloying effects and dissolve second phases in the mother alloys.^{26–28} Mixing two phases mechanically into a single phase solid solution was not possible by conventional cold-rolling in the previous study. In the present study, a SPD process was applied to CoCrCuFeNi to mix the two FCC phases to produce a single phase solid solution, or at least to make the microstructure more homogeneous. Among the SPD processes for obtaining ultrafine-grained metallic materials,^{29–33} such as equal channel angular extrusion, accumulative roll bonding and high pressure torsion (HPT), the HPT process allows much higher plastic strains than the other processes without fracture of the samples, because of the large hydrostatic compressive stress applied to the specimens in HPT. This study discusses the mechanical property and microstructure of a CoCrCuFeNi system processed by HPT at ambient temperatures and then annealed at various temperatures.

EXPERIMENTAL PROCEDURES

The alloy used in the present study was Co₂₁Cr₂₂Cu₂₂Fe₂₁Ni₁₄ in atomic percent, which was the same alloy used in the previous study.^{20,21} An ingot, 10 mm in diameter and 60 mm in length, was

cast using a pseudo-float melting process. The ingot was homogenized at 1100°C for 12 h in a vacuum furnace, followed by water cooling (called the *starting material* hereafter). The starting material was cut into a disk, 10 mm in diameter and 0.8 mm in thickness. The disk-shaped specimen was subjected to the HPT process at ambient temperature under 7.5 GPa at a speed of 0.2 rpm. The rotation angles of HPT to study the deformation behaviors were 5°, 90°, 180°, 360°, and 1800°. The specimens, HPT processed to 1800°, were annealed at 500°C, 550°C, 600°C, and 650°C for 30 min to examine the annealing behaviors.

The microstructures of the HPT processed and annealed specimens were observed by field-emission scanning electron microscopy (SEM) with a backscattered electron (BSE) detector. Transmission electron microscopy (TEM) was also used to observe the microstructures of the annealed specimens, which were prepared by mechanical polishing, electro-polishing in a solution containing 10% HClO₄ and 90% CH₃COOH at 25°C, and final ion milling at 5 kV. A Vickers microhardness test was carried out on at least five points on the same strain region in a HPT processed specimen with a dwelling time of 15 s. Cross-sections perpendicular to the radial direction of the disks were used for the microstructural observations by BSE-SEM and also for the microhardness measurements. X-ray diffraction (XRD) using Cu-K α_1 at 45 kV and 40 mA was performed to identify the phases in the material. Three-dimensional atom probe tomography (APT) was performed using a local electrode atom probe (LEAP 4000X HRTM; CAMECA Instruments) with a voltage pulse mode at 50 K. The APT sample was prepared using a dual beam focused-ion-beam, and a low energy (5 keV) Ga beam was used at the final milling stage to remove the contaminated layers.

RESULTS AND DISCUSSION

Strengthening During HPT Process

Figure 1 is a BSE-SEM image of the starting material of the Co₂₁Cr₂₂Cu₂₂Fe₂₁Ni₁₄ system. The starting material showed a typical solidified structure. Two face-centered cubic structured phases were observed in the as-cast material:²⁰ the matrix is a Cu-lean phase and the other is a Cu-rich phase (dark region) distributed at the grain boundary and grain interior of the Cu-lean phase, as indicated by the arrows. The average microhardness of the starting material was 190 HV. The starting material was subjected to the HPT process with different rotation angles at ambient temperature. Figure 2 shows the change in microhardness of the HPT processed specimens. The microhardness increased gradually with increasing rotation angle and distance from the center of the disk. The shear strain (γ) in torsion was calculated using the following equation:

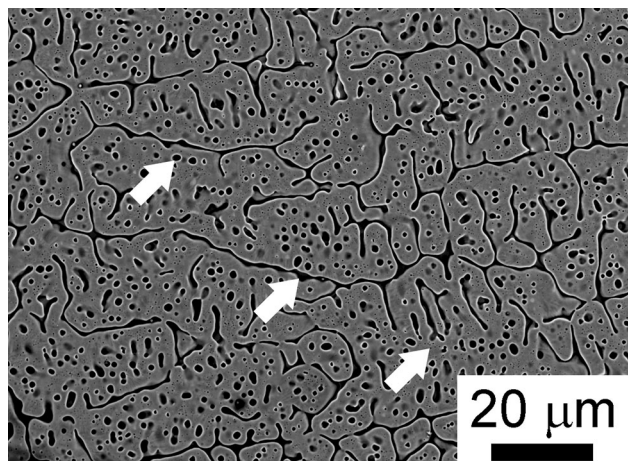


Fig. 1. BSE-SEM image of the starting material. Cu-rich regions with various sizes distributed at the grain boundary and grain interior of the matrix are indicated by arrows.

$$\gamma = \theta \frac{d}{t}, \quad (1)$$

where θ is the rotation angle in radians, d is the distance from the center of the disk and t is the thickness of the disk (0.8 mm in the present study). The difference in hardness within each specimen shown in Fig. 2a was attributed to the difference in shear strain at different radial positions within the disk. The microhardness shown in Fig. 2a are plotted in Fig. 2b as a function of the shear strain. The microhardness increased gradually with increasing shear strain, which confirmed that the hardness can be understood basically by the applied strain. In Fig. 2b, there are two stages in the hardness change. When the shear strain was above 20, the slope of microhardness change was higher than that below a strain of 20. To understand the strengthening mechanism in the $\text{Co}_{21}\text{Cr}_{22}\text{Cu}_{22}\text{Fe}_{21}\text{Ni}_{14}$ system during HPT, microstructural observations were carried out on the specimens HPT processed by various rotation angles (i.e., various strains).

Figure 3 shows BSE-SEM images of the specimens HPT processed to different rotation angles ranging from 5° to 1800° . The place at which the microstructures were observed was 4 mm from the center of the disk, so that the corresponding shear strains in Fig. 3a–d are 0.44, 15.7, 31.4, and 157, respectively. The shear direction of torsion is parallel to the horizontal axis of each image. The Cu-rich (dark) regions are pointed by the arrows in the figures. Under a pressure of 7.5 GPa in HPT, the specimen was compressed to the vertical direction, but the compression reduction was only 6.3%. As a result, the grains were elongated along the horizontal direction (shear direction) after 5° rotation, as shown in Fig. 3a. The Cu-rich region still appeared clear at the grain boundary or grain interior of the matrix. With increasing rotation angle, the grains were increasingly elongated and

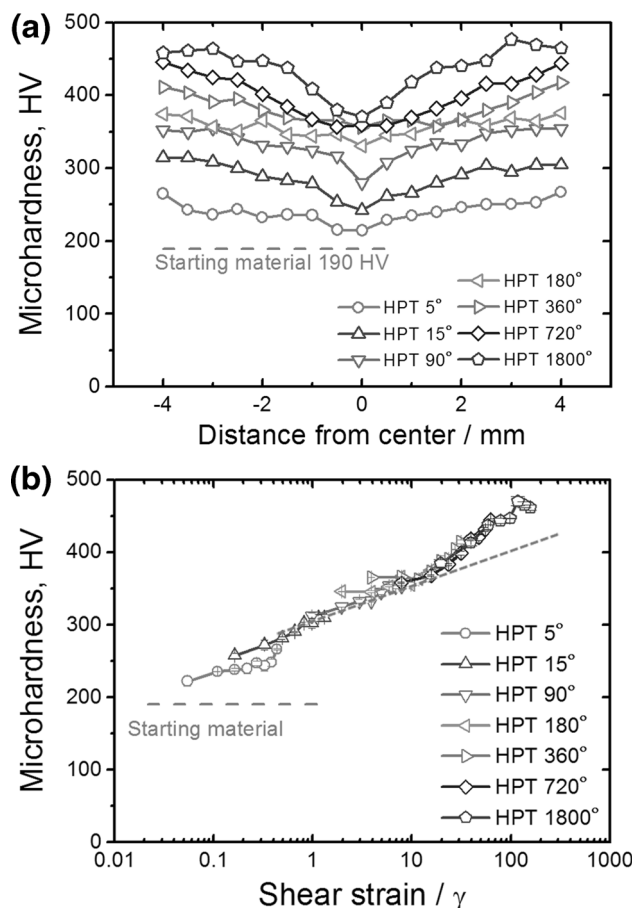


Fig. 2. Change in the microhardness of the specimens HPT processed at different rotation angles. Plotted as a function of (a) the distance from the center of the disk and (b) shear strain (γ).

become thinner. Therefore, a large increase in the interface areas between the Cu-rich phase and Cu-lean matrix is expected. As shown in Fig. 3b and c, the distance between the Cu-rich phases becomes much closer than that in Fig. 1 or 3a. After 1800° rotation of HPT, the distance between the Cu-rich phases was less than 100 nm. The microstructural geometry of the material was changed greatly by HPT deformation concomitantly with the accumulation of dislocations and other lattice defects corresponding to a significant increase in hardness shown in Fig. 2.

Figure 4 presents XRD patterns of the starting material and the specimens HPT processed at different rotation angles. The starting material consisted of two FCC phases: a Cu-lean matrix (FCC1) and a Cu-rich second phase (FCC2) with lattice parameters of 0.35859 nm and 0.36148 nm, respectively.²⁰ With increasing rotation angle in HPT, the intensity of the (200) peak decreased, whereas that of the (111) peak increased to form a torsion deformation texture (shear texture). Figure 4b presents an enlarged part of Fig. 4a, making it possible to see how much the two (111) peaks merged with each other. Two (111) peaks were clearly distinguished

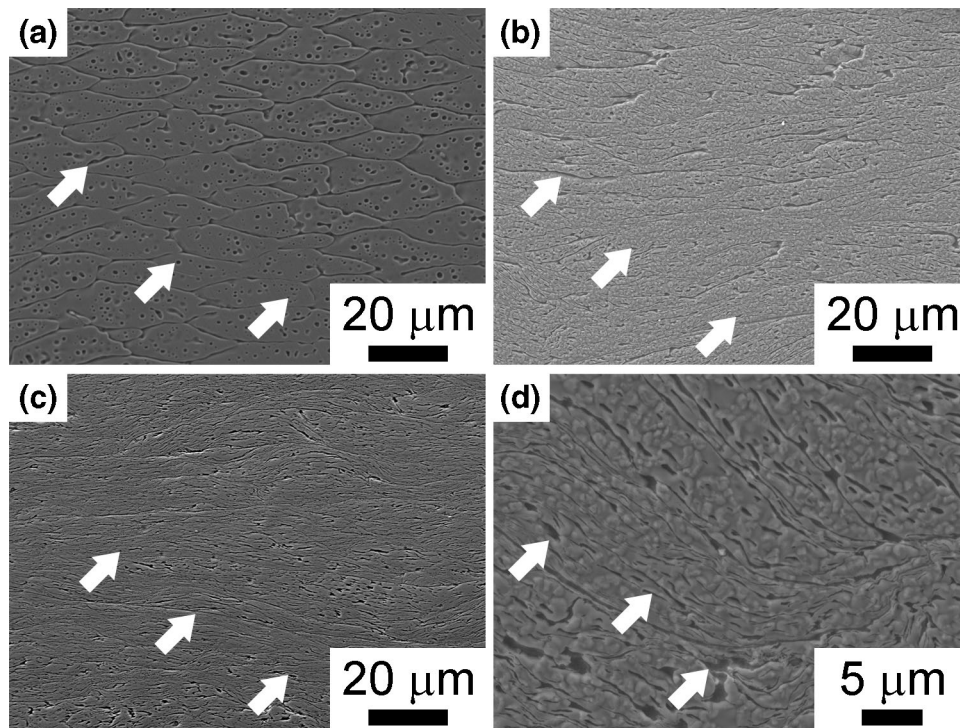


Fig. 3. BSE-SEM images of the specimens HPT processed at different rotation angles: (a) 5°, (b) 180°, (c) 360° and (d) 1800°, so that the corresponding shear strains are 0.44, 15.7, 31.4 and 157.1, respectively. The shear direction in torsion is parallel to the horizontal axis of each image.

when the rotation angle of HPT was smaller than 360°. On the other hand, the two peaks could no longer be clearly distinguished when the specimens were subjected to the HPT process with rotation angles larger than 360°. Note that the center of the (111) peak of the Cu-lean matrix is shifted to a lower angle in the 1800° HPT specimen, indicating an increase in the lattice parameter during the HPT process. Although the conclusion that the two phases are mixed during HPT is premature, the result suggests that a large amount of the Cu-rich phase might have dissolved into the Cu-lean matrix, leading to an increase in the lattice parameter of the Cu-lean phase. In addition, such dissolution of the Cu-rich phase into the Cu-lean matrix might contribute to the increase in hardness observed in Fig. 2b through solid solution hardening, particularly when the shear strain was above 20. Therefore, there are at least three strengthening mechanisms in $\text{Co}_{21}\text{Cr}_{22}\text{Cu}_{22}\text{Fe}_{21}\text{Ni}_{14}$ system during the HPT process: dislocation hardening generated by plastic deformation, grain refinement strengthening realized by SPD, and solid solution hardening of Cu caused by dissolution of the Cu-rich phase into the Cu-lean matrix.

Strengthening During Annealing Process

This section discusses strengthening mechanisms of $\text{Co}_{21}\text{Cr}_{22}\text{Cu}_{22}\text{Fe}_{21}\text{Ni}_{14}$ system during annealing at different temperatures. The specimens HPT

processed to a rotation angle of 1800° were annealed at 500°C, 550°C, 600°C, and 650°C for 30 min, as mentioned previously. Figure 5 shows the change in microhardness of the annealed specimens. The open square symbols are the values of the as-HPT processed specimen without heat treatment. The microhardness of the specimen annealed at 650°C was softer than the others. On the other hand, the specimens annealed at 550°C and 600°C were strengthened by the heat treatment.

Figure 6 shows the XRD pattern of the specimens annealed at different temperatures, together with that of the as-HPT processed specimen. Figure 6b is an enlarged part of Fig. 6a. When the specimen was annealed at 650°C, two (111) peaks corresponding to two FCC phases appeared separately, whereas a single (111) peak was observed when the specimens were annealed at temperatures lower than 650°C.

A fully recrystallized microstructure was observed in the specimens annealed at 600°C and 650°C. Figure 7a presents a SEM-BSE image of the specimen annealed at 600°C, and Fig. 7b shows a TEM of the specimen annealed at 650°C. These micrographs corresponded to the highest and lowest microhardness values in Fig. 5, respectively. As shown in Fig. 7a, an equiaxed grain structure was observed in the 600°C annealed specimen, and the grain size of the specimen annealed at 600°C was much finer than 100 nm. In addition, there were a number of dark particles smaller than 20 nm inside the matrix grains, which are believed to be Cu-rich precipitates

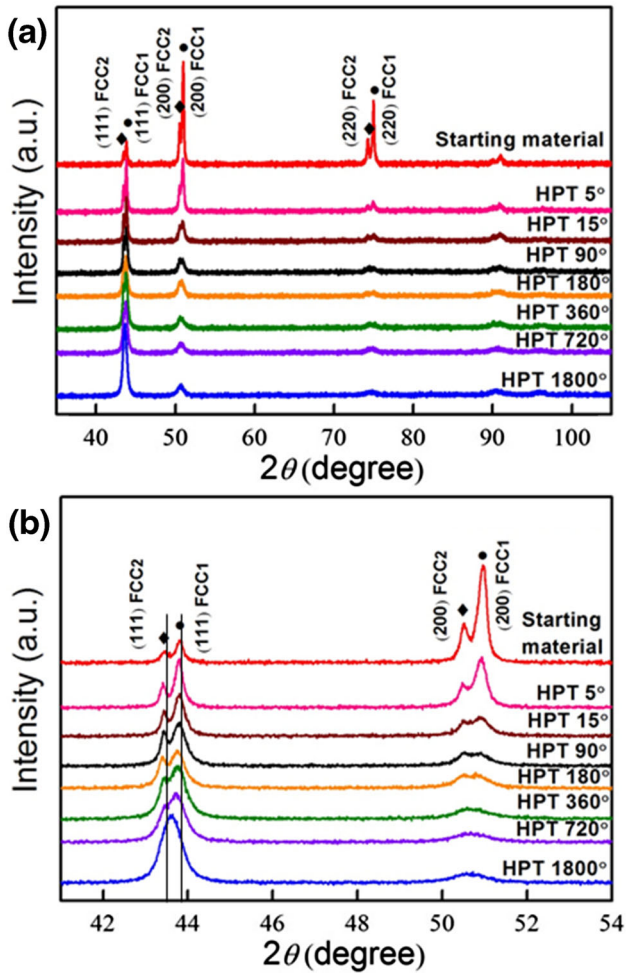


Fig. 4. X-ray diffraction patterns of the specimens HPT processed at different rotation angles: (a) full range and (b) enlarged part of (a).

re-precipitated from a supersaturated solid solution formed by SPD (HPT). On the other hand, the microstructure of the specimen annealed at 650°C (Fig. 7b) had no dark and fine particles but only equiaxed grains with a mean grain size of 110 nm.

The recrystallization temperature of the 90% cold-rolled $\text{Co}_{21}\text{Cr}_{22}\text{Cu}_{22}\text{Fe}_{21}\text{Ni}_{14}$ system was reported to be between 600°C and 650°C.²⁰ This is also close to half the melting temperature of the $\text{Cr}_{20}\text{Fe}_{20}\text{Co}_{20}\text{Ni}_{20}\text{Cu}_{20}$ system in Kelvin,³⁴ which is similar to the typical recrystallization temperatures of conventional metallic materials. As the material was heavily deformed by HPT in the present study, it is natural that the recrystallization temperature of the alloy would be lower than that reported before. As shown in Fig. 7, fully recrystallized microstructures of the specimens annealed at 600°C and 650°C suggest that the effect of dislocation hardening is removed, which also coincides with the sharpness of the XRD peaks after annealing in Fig. 6. The reason for the softening in the specimen annealed at 650°C might be coarsening of the Cu-rich phase during annealing, as shown in the split

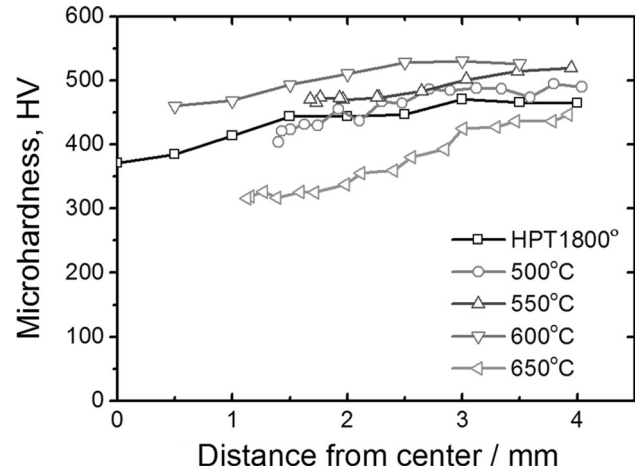


Fig. 5. Change in the microhardness of the specimens annealed at 500°C, 550°C, 600°C, and 650°C for 1.8 ks. Plotted as a function of the distance from the center of the disk.

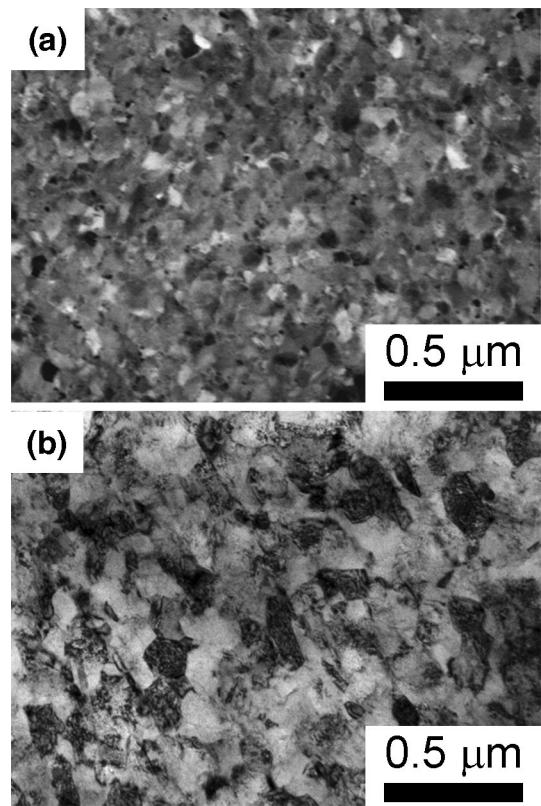


Fig. 6. X-ray diffraction patterns of the specimens annealed at different temperatures: (a) full range and (b) enlarged part of (a).

XRD pattern in Fig. 6b. As reported previously, Cu tends to form a Cu-rich phase, as shown in Fig. 1, because of its positive mixing enthalpy with other elements in the present system²⁰ when the temperature was high enough for Cu diffusion. Therefore, the enrichment of Cu produces Cu-rich clusters, but the other grains are depleted with Cu. As shown in Fig. 6b, separate (111) peaks

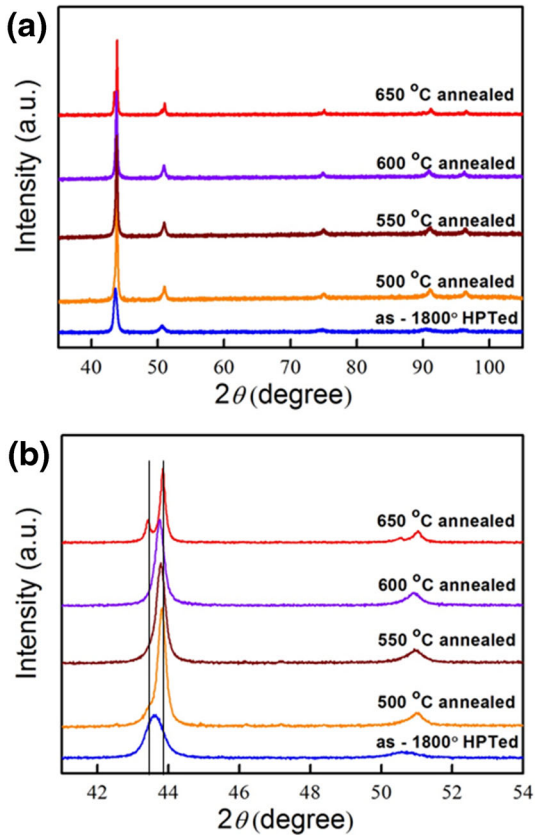


Fig. 7. Microstructures of the specimens annealed for 30 min at (a) 600°C and (b) 650°C. The micrographs were taken by (a) BSE-SEM and (b) TEM.

corresponding to the two FCC phases were clearly observed after annealing at 650°C, indicating that the Cu-rich phase has a sufficient volume fraction.

The 600°C annealed specimen was analyzed by APT to understand the effects of the precipitates (dark particles) on strengthening in the specimen annealed at 600°C in Fig. 7a. Figure 8 shows the APT result of the specimen annealed at 600°C. Figure 8a–e presents the single element distribution maps of Co, Fe, Ni, Cr, and Cu, respectively. The inhomogeneous distribution of Cu was clearly seen in Fig. 8e, in which the isosurface of Cu (>50 at.%) is shown to make the Cu-rich or Cu-depleted areas clearer. The dashed line is a trace of the APT tip, and a region of interest (ROI) is marked with a thin pink tube in Fig. 8f. The one-dimensional Cu profile along the longitudinal direction of the ROI is displayed in Fig. 8g. As shown in Fig. 8f, the size of the isosurface of spheroidized Cu ranged from approximately 2–32 nm, indicating that the dark particles observed in Fig. 7a were Cu-rich clusters. Based on the results mentioned above, the phenomena observed in the specimen annealed at 600°C can be explained

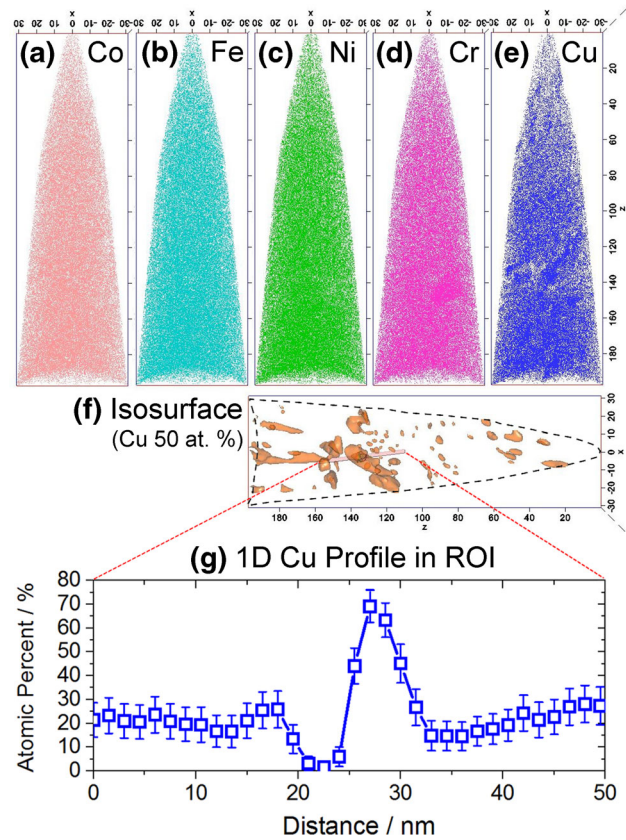


Fig. 8. 3D APT results of the specimen annealed at 600°C. (a)–(e): distribution of (a) Co, (b) Fe, (c) Ni, (d) Cr and (e) Cu. (f) Isosurface of Cu (above 50 at.%) and a region of interest (rectangular). (g) Cu concentration profile along the pink line in (f).

by the mechanically dissolved Cu atoms in the matrix during the HPT process being clustered or precipitated again during the low temperature annealing process, forming nano-precipitates (dark particles in Fig. 7a). Cu-rich nano-precipitates form because the diffusion of Cu atoms is still limited at 600°C, and the diffusion length of Cu is limited for a given period of annealing (1.8 ks). Such nano-precipitates with sizes of 2–32 nm act as obstacles for the dislocation slip, increasing the strength of the specimens. Fine precipitates also pin the grain growth of the matrix, reserving grain refinement strengthening.

Although this study attempted to unveil deformation and recrystallization behavior of $\text{Co}_{21}\text{Cr}_{22}\text{-Cu}_{22}\text{Fe}_{21}\text{Ni}_{14}$ system, several issues remain unclear. For example, the change in microhardness during the HPT process shown in Fig. 5 has not yet been saturated, even at a shear strain of 157. Dissolution of the Cu-rich second phase was not proven directly, and the re-precipitation behaviors at 550°C and 500°C annealing were not studied. A further systematic study will be necessary to understand the deformation and recrystallization behaviors of the CoCrCuFeNi system.

SUMMARY AND CONCLUSION

This study examined the microstructure and mechanical property of $\text{Co}_{21}\text{Cr}_{22}\text{Cu}_{22}\text{Fe}_{21}\text{Ni}_{14}$ system processed by HPT and subsequent annealing. Based on the microstructure evolution, microhardness changes and APT, the following major results were obtained:

1. As shear strain applied in HPT was increased to 157, the microhardness increased from 190 HV to 470 HV. When the shear strain was above 20, the slope of the microhardness change was higher than that below a strain of 20. The change in the slope might be due to dissolution of the Cu-rich phase into the Cu-lean matrix.
2. The microhardness of the specimens annealed at temperatures lower than 650°C increased to 540 HV, which was much higher than the hardness of the as-HPT processed specimen. This was attributed to the re-precipitation of Cu-rich nano-particles with sizes of 2–32 nm in the matrix, which was confirmed by APT analysis.
3. The microhardness of the specimen annealed at 650°C was significantly decreased due to the absence of Cu-rich nano-particles in the matrix, but the coarsening of equiaxed grains with a mean grain size of 110 nm was observed.

ACKNOWLEDGEMENT

This study was supported financially by the Grant-in-Aid for Scientific Research on Innovative Area, “Bulk Nanostructured Metals” (Area No. 2201), the Grant-in-Aid for Scientific Research (A) (No. 24246114), the Grant-in-Aid for Challenging Exploratory Research (No. 26630365), and the Elements Strategy Initiative for Structural Materials (ESISM), all through the Ministry of Education, Culture, Sports, Science and Technology (MEXT), Japan (Contact No. 22102002). All the support is gratefully appreciated.

REFERENCES

1. J.-W. Yeh, S.-K. Chen, S.-J. Lin, J.-Y. Gan, T.-S. Chin, T.-T. Shun, C.-H. Tsau, and S.-Y. Chang, *Adv. Eng. Mater.* 6, 299 (2004).
2. J.-W. Yeh, *JOM* 65, 1759 (2013).
3. K. Zhang and Z. Fu, *Intermetallics* 22, 24 (2012).
4. M.C. Gao, *JOM* 66, 1964 (2014).
5. W.H. Liu, Y. Wu, J.Y. He, T.G. Nieh, and Z.P. Lu, *Scr. Mater.* 68, 526 (2013).
6. F. Otto, A. Dlouhý, C. Somsen, H. Bei, G. Eggeler, and E.P. George, *Acta Mater.* 61, 5743 (2013).
7. M.J. Yao, K.G. Pradeep, C.C. Tasan, and D. Raabe, *Scr. Mater.* 72–73, 5 (2014).
8. Y. Zhang, T.T. Zuo, Z. Tang, M.C. Gao, Z.P. Lu, P.K. Liaw, and K.A. Dahmen, *Prog. Mater. Sci.* 61, 1 (2014).
9. W. Ji, W. Wang, H. Wang, J. Zhang, Y. Wang, F. Zhang, and Z. Fu, *Intermetallics* 56, 24 (2015).
10. C. Zhu, Z.P. Lu, and T.G. Nieh, *Acta Mater.* 61, 2993 (2013).
11. Z. Wu, H. Bei, F. Otto, G.M. Pharr, and E.P. George, *Intermetallics* 46, 131 (2014).
12. B. Schuh, F. Mendez-Martin, B. Völker, E.P. George, H. Clemens, R. Pippin, and A. Hohenwarter, *Acta Mater.* 96, 258 (2015).
13. K.-Y. Tsai, M.-H. Tsai, and J.-W. Yeh, *Acta Mater.* 61, 4887 (2013).
14. M.C. Gao, *JOM* 65, 1749 (2013).
15. Y. Zhang, Y.J. Zhou, J.P. Lin, G.L. Chen, and P.K. Liaw, *Adv. Eng. Mater.* 10, 534 (2008).
16. A. Takeuchi and A. Inoue, *JIM Mater. Trans.* 41, 1372 (2000).
17. F. Zhang and U. Kattner, *J. Phase Equilib. Diffus.* 36, 1 (2015).
18. A. Durga, K.C. Hari Kumar, and K.C. BS, *Trans. Indian Inst. Met.* 65, 375 (2012).
19. F. Zhang, C. Zhang, S.L. Chen, J. Zhu, W.S. Cao, and U.R. Kattner, *CALPHAD* 45, 1 (2014).
20. N. Park, I. Watanabe, D. Terada, Y. Yokoyama, P.K. Liaw, and N. Tsuji, *Metall. Mater. Trans. A* 46, 1481 (2015).
21. N. Park, I. Watanabe, D. Terada, Y. Yokoyama, P.K. Liaw, and N. Tsuji, *Metall. Mater. Trans. A* 46, 3308 (2015).
22. E. Botcharova, M. Heilmaier, J. Freudenberger, G. Drew, D. Kudashov, U. Martin, and L. Schultz, *J. Alloys Compd.* 351, 119 (2003).
23. C. Suryanarayana, *Prog. Mater. Sci.* 46, 1 (2001).
24. K. Uenishi, K.F. Kobayashi, K.N. Ishihara, and P.H. Shingu, *Mater. Sci. Eng. A* 134, 1342 (1991).
25. J. Xu, U. Herr, T. Klassen, and R.S. Averbach, *J. Appl. Phys.* 79, 3935 (1996).
26. S. Ohsaki, S. Kato, N. Tsuji, T. Ohkubo, and K. Hono, *Acta Mater.* 55, 2885 (2007).
27. X. Sauvage, F. Wetscher, and P. Pareige, *Acta Mater.* 53, 2127 (2005).
28. Y.F. Sun, H. Fujii, T. Nakamura, N. Tsuji, D. Todaka, and M. Umamoto, *Scr. Mater.* 65, 489 (2011).
29. R.Z. Valiev, R.K. Islamgaliev, and I.V. Alexandrov, *Prog. Mater. Sci.* 45, 103 (2000).
30. N. Tsuji, Y. Ito, Y. Saito, and Y. Minamino, *Scr. Mater.* 47, 893 (2002).
31. J.A. Wert, X. Huang, G. Winther, W. Pantleon, and H.F. Poulsen, *Mater. Today* 10, 24 (2007).
32. S. Khamsuk, N. Park, H. Adachi, D. Terada, and N. Tsuji, *J. Mater. Sci.* 47, 7841 (2012).
33. M. Joshi, Y. Fukuta, S. Gao, N. Park, D. Terada, N. Tsuji, and I.O.P. Conf, *Ser. Mater. Sci. Eng.* 63, 012074 (2014).
34. C.-J. Tong, Y.-L. Chen, J.-W. Yeh, S.-J. Lin, S.-K. Chen, T.-T. Shun, C.-H. Tsau, and S.-Y. Chang, *Metall. Mater. Trans. A* 36, 881 (2005).